

Fatigue-caused damage in trabecular bone from clinical, morphological and mechanical perspectives

Mirzaali Mazandarani, Mohammad; Libonati, F.; Böhm, C.; Rinaudo, L.; Cesana, B. M.; Olivieri, F. M.; Vergani, L.

DOI

[10.1016/j.ijfatigue.2019.105451](https://doi.org/10.1016/j.ijfatigue.2019.105451)

Publication date

2020

Document Version

Final published version

Published in

International Journal of Fatigue

Citation (APA)

Mirzaali Mazandarani, M., Libonati, F., Böhm, C., Rinaudo, L., Cesana, B. M., Olivieri, F. M., & Vergani, L. (2020). Fatigue-caused damage in trabecular bone from clinical, morphological and mechanical perspectives. *International Journal of Fatigue*, 133, Article 105451. <https://doi.org/10.1016/j.ijfatigue.2019.105451>

Important note

To cite this publication, please use the final published version (if applicable). Please check the document version above.

Copyright

Other than for strictly personal use, it is not permitted to download, forward or distribute the text or part of it, without the consent of the author(s) and/or copyright holder(s), unless the work is under an open content license such as Creative Commons.

Takedown policy

Please contact us and provide details if you believe this document breaches copyrights. We will remove access to the work immediately and investigate your claim.



Fatigue-caused damage in trabecular bone from clinical, morphological and mechanical perspectives

M.J. Mirzaali^{a,b}, F. Libonati^a, C. Böhm^a, L. Rinaudo^c, B.M. Cesana^d, F.M. Ulivieri^e, L. Vergani^{a,*}

^a Department of Mechanical Engineering, Politecnico di Milano, Via La Masa 1, 20156 Milano, Italy

^b Department of Biomechanical Engineering, Faculty of Mechanical, Maritime, and Materials Engineering, Delft University of Technology (TU Delft), Mekelweg 2, 2628 CD, Delft, The Netherlands

^c Technologic s.r.l., Torino, Italy

^d University of Milan, Milan, Italy

^e Fondazione IRCCS Cà Granda Ospedale Maggiore Policlinico, UO Nuclear Medicine-Bone Metabolic Unit, Milano, Italy

ARTICLE INFO

Keywords:

Fatigue loading
Bone damage
Trabecular bone score
Bone mineral density
 μ CT-imaging

ABSTRACT

Bone quantity and quality are considered the main predictors of bone mechanical properties (*i.e.*, strength and fracture resistance). These factors deal with the morphology and chemical composition of bone and can be assessed by non-invasive techniques such as dual-energy x-ray absorptiometry (DXA), providing the bone mineral density (BMD) and the trabecular bone score (TBS). These parameters, and in particular BMD, are currently used as clinical predictors of fracture risk but do not provide information regarding the fatigue life. Bone is continuously subjected to fatigue loading and fatigue-induced damage can be crucial in fragility fractures. To probe the effect of fatigue-induced damage on bone microarchitecture and elucidate the effect of such damage on the bone clinical parameters, we combined fatigue testing on *ex-vivo* porcine trabecular bone samples with DXA measurements and μ CT imaging. In addition, we performed interrupted cyclic tests at different load levels and measured fatigue-induced damage accumulation in the form of stiffness degradation. We also highlighted the change of clinical and microstructural parameters during the accumulation of fatigue-induced damage in interrupted fatigue tests. Our results suggest that the parameters obtained from the current non-invasive diagnostic protocols (*i.e.* μ CT and DXA) are not able to assess the amount of fatigue-induced damage. This can be due to the fact that such techniques provide global parameters, whereas fatigue-induced damage is a local phenomenon, closely connected to the microarchitecture.

1. Introduction

Bone provides support to human and animal bodies, also protecting organs and enabling mobility. It is well known that aging and diseases or traumatic events [1–3] or static and fatigue loadings [4] significantly affect the fracture resistance of bone. Yet, it is not completely understood whether bones have more tendency to fracture due to fatigue or static loadings [5]. The first clear evidence of fatigue-induced fractures emerged about one century ago [1–3] when fractures occurred in athletes [6] or military recruits [7] exposed to periods of long and hard training. Currently, another type of fatigue-induced fracture is becoming more common owing to an ever-aging population. In healthy bones, accumulation of microdamage under cyclic loading is a slow process, which also stimulates the remodeling, promoting repair [5]. Conversely, in elder or osteoporotic bones (*i.e.*, a bone disease with significant bone loss) the faster growth of fatigue microdamage or the

slower repair causes failures [8]. Accumulation of microcracks and diffuse damage, which are the consequences of both single static overloading events [9–17] and repetitive physiological loadings [2,18–22] can lead to the degradation of mechanical properties [11,23–26]. Understanding the different kinds of damage and their effect on bone strength and life is complex, yet, the knowledge of the fatigue behavior of bones has become a paramount concern owing to the population's longer lifespan.

Fatigue-induced damage can impair bone strength and play a crucial role in fragility fractures. *In-vivo* fatigue (destructive) testing are precluded and *ex-vivo* experiments are generally used to evaluate fatigue-induced damage for bones. Previous studies have addressed this topic considering the whole vertebra [27] or focusing on the cortical bone [22,28–30]. Few studies [31,32] focused on the fatigue behavior of the cancellous tissue showing that the fatigue curve (S-N curve) of trabecular bone tissue is not dependent on the site and the species [31],

* Corresponding author at: Department of Mechanical Engineering, Politecnico di Milano, Via G. La Masa 1, 20156 Milano, Italy.

E-mail address: laura.vergani@polimi.it (L. Vergani).

and that the fatigue strength is correlated with age and BMD (bone mineral density) [32].

Today, the most widely adopted clinical parameters for the assessment and prediction of bone fracture risk are BMD and TBS (Trabecular Bone Score [33–35]) measured via the dual-energy x-ray absorptiometry (DXA) and bone quantity and quality, respectively. Although BMD and TBS are currently used as predictors of bone fragility [36–38], there is no clear evidence of significant correlation between these parameters and the fatigue life. Also, it is not clear how these parameters are affected by cyclic loading and fatigue-induced damage. A low BMD is generally considered a predictor of bone fragility. Yet, both younger and more senior individuals with the same level of BMD have shown different fracture risks [39,40] and over half of all non-vertebral fractures observed in people above 55 occurred to those with a normal BMD [41]. Thus, bone quality, which can be influenced by the amount of microdamage and its accumulation with aging [19], can also play a crucial role in the occurrence of bone fatigue fractures [42,43].

In this study, to demonstrate the effect of fatigue-induced damage on both the 3D-bone microarchitecture and the bone clinical parameters, we combined fatigue testing under uniaxial compressive loading on *ex-vivo* porcine trabecular bone samples with DXA measurements and μ CT imaging. Additionally, we performed interrupted cyclic loading at different load levels, to highlight the life-trend of the microstructural and clinical parameters. We hypothesized that fatigue-induced continuum damage in the form of stiffness degradation is significantly correlated to the microarchitectural morphology of trabecular bone. Moreover, based on Wöhler analysis, we developed two fatigue models accounting for the following parameters: *i*) specimen-specific effective area, measured via μ CT, *ii*) specimen-specific initial elastic modulus, and *iii*) BMD.

The choice of testing porcine vertebrae was motivated by the fact that the morphology is similar to the human one [44] and spines are amongst the skeletal sites, which are more commonly affected by fractures.

2. Materials and methods

We focused on trabecular tissue taken from porcine vertebrae of similar age and weight and unknown sex. The experimental procedures followed in this study are listed below and described in different subsections:

- (1) Sample preparations from lumbar vertebrae taken from porcine lumbar spines;
- (2) Analysis of undamaged samples via
 - (a) DXA scanning;
 - (b) μ CT imaging;
- (3) Mechanical testing on bone samples
 - (a) Preliminary quasi-static compression tests, to obtain an initial indication of the appropriate force amplitudes and to define the stop criterion in the fatigue tests;
 - (b) High-cycle fatigue tests;
 - (c) Interrupted cyclic tests followed by DXA scanning and μ CT imaging;
- (4) Statistical analysis;

Thirty specimens were tested in this study and divided into three groups, *i.e.* three specimens for the quasi-static compression tests, twenty-one specimens for fatigue tests and six specimens for the interrupted cyclic tests. One specimen, subjected to interrupted cyclic loading (force level 360 N), was removed from the data analysis due to catastrophic damage during the test.

2.1. Sample preparation

Six porcine lumbar spines with six lumbar vertebrae (L1 to L6) were

collected from a local butcher. The spines belonged to 12–18-month-old animals, of unknown sex, and about 120 kg weight. The spines were stored at $-18\text{ }^{\circ}\text{C}$ until sample preparation and experimental tests. Each vertebra was separated from the spine by handsaw cutting at the inter-vertebral discs. Using a manual hand drill, a cylindrical specimen (diameter, D , 16 mm and length 35 mm) was cored out of each vertebra, along the vertebrae axis. The bone sample was then transferred to a lathing machine to reduce the diameter, D , to 14 mm. The length of the specimen, L_0 , was reduced to 22 mm with a circular saw (Hitech Europe, rpm = 1000 min^{-1}). During the preparation steps, the specimens were kept hydrated by adding the saline solution. Thirty cylindrical specimens were prepared for mechanical testing. To eliminate the boundary effects and improve the force transmission, the specimens were glued into custom-made aluminum end caps using Loctite 496®. Before the adhesive bonding was applied, the end caps were cleaned for about two minutes in an ultrasonic bath, then rinsed with acetone. The internal surfaces of the end caps were roughened using sandpaper (grit size #320) to increase the bonding strength between the internal surface of the end caps and the bone tissue. Both ends of the bone specimens were defatted with the acetone before glueing. After glueing the bone specimen ends into the end caps, the samples were kept at ambient temperature for 24 h to ensure a complete curing of the glue. Finally, the specimens were frozen again at $-18\text{ }^{\circ}\text{C}$ until the next steps. The end caps, having an internal diameter of 14 mm and an external diameter of 20 mm, covered 3 mm of the cylindrical-shape specimens. The effective length between the gripping holders was $L_{eff} \approx 16\text{ mm}$.

2.2. Analysis of undamaged samples

2.2.1. DXA scanning

DXA scanning was performed on the trabecular bone specimens at the Bone Metabolic Unit of Nuclear Medicine of the Fondazione IRCCS Ca' Granda-Ospedale Maggiore Policlinico, using a Hologic Discovery A system (Hologic Inc, Marlborough, Massachusetts, USA, software version: 13.3.0.1.3). BMD was measured through the APEX software installed on the same machine. TBS was automatically calculated using the software provided by the Medimaps Group (Wilmington, US) and on the same machine. The scans were performed using the posterior-anterior lumbar spine option with a pixel size of $0.5 \times 0.5\text{ mm}^2$. Four trabecular bone specimens were placed in the scanning machine in each batch, and the total scanning time was about two minutes. The samples were kept frozen ($-18\text{ }^{\circ}\text{C}$) before and after scanning, to prevent any deterioration of the bone microstructure. In a post-processing analysis, BMD and TBS were calculated by the manual selection of the region of interest of the bone scans. This setup resulted in the exclusion of the aluminum stand from the bone scans. The segmentation method in DXA scanning being a manual procedure, we performed the measurement three times to evaluate the segmentation effect on our results. From each set of scans, BMD and TBS were obtained for the bone specimens. DXA scanning was performed on all the samples before and after the mechanical fatigue tests, and at the beginning of each interrupted fatigue step.

2.2.2. μ CT imaging

μ CT imaging of the bone specimens was performed on trabecular bone specimens using an X-ray Metrology CT system (X25, North Star Imaging Inc., Buckinghamshire, UK) with the spatial resolution of 25.6 μm . The scanning parameters were fixed at 60 kV and 150 μA . Three specimens, submerged in the saline solution, were placed simultaneously in the scanning machine and each scan took 110 min. Image reconstruction was performed with the x-view CT software. Post-processing of the images was carried out using ImageJ [45] and BoneJ plugin [46]. A Gaussian blur filter (standard deviation of the Gaussian distribution 1.5) was used to remove the noise from the images. Afterward, the scans were converted to gray-level 8-bit images. The gray-level images were segmented by the Otsu local thresholding

method [47], resulting in binary images with the voxel value of 1, for bone, and 0, for the empty spaces.

Conventional morphological parameters were calculated for each specimen for a cylindrical region of interest (ROI). These parameters included: bone density ($BV/TV = \frac{\text{bone volume}}{\text{total volume}}$); bone porosity, ($\rho_p = 1 - \frac{BV}{TV}$); trabecular thickness ($Tb.Th$) and trabecular spacing ($Tb.Sp$), calculated based on the conventional definition of the greatest sphere that fits within the structure [48]; bone surface (BS), defined as the inner surface of the bone material and calculated by the summation of the triangulated mesh area obtained from the isosurface creation (with a resampling equal to 1) [49]; trabecular ellipsoid factor ($Tb.EF$), which locally distinguishes between rod- or plate-like trabeculae [50]; connectivity density ($Conn.D.$), which determines the number of 3D-connected trabeculae; the degree of anisotropy (DA), which defines the main microstructural orientation of bone [51,52]

2.3. Mechanical testing

2.3.1. Quasi-static compression tests

Three specimens were tested under monotonic compression loading (MTS machine Alliance, RF/150 with a load cell of 150 kN, class 1 ISO 7500-1) to obtain the yield stresses and strains based on the 0.2%-strain criterion. In the light of these results, a displacement stop criterion, equal to 2 mm, was set to end the fatigue tests. The corresponding yield forces were calculated from the measured yield stresses. A typical force-displacement curve for the monotonic compression tests is shown in Fig. S1 of the supplementary document.

2.3.2. Fatigue tests

High-cycle fatigue (HCF) testing was performed under force control using an MTS 810 servo-hydraulic testing system equipped with an MTS 661.20F-03 load cell (maximum load capacity 100 kN), with an accuracy of 20 N. The fatigue testing time being demanding, we created a proper testing environment: during loading, specimens were submerged in saline solution (NaCl 0.9%) using a custom-designed aquarium. The gripping set-up was endowed with a pressure disc and pressure stamp. The pressure disc had a polished and greased spherical surface fitted to the pressure stamp. Three circumferential pre-tension springs were used to pull the pressure disc into the stamp. This allowed the pressure disc to be moved before the test and to be adaptively aligned to the specimens during mechanical testing. It also resulted in smooth force transmission and reduced peak stress, due to partial contact between the end cap and the pressure disc surfaces.

After performing the preliminary tests, we set a load frequency of 10 Hz, which is higher than the frequency of normal walking (*i.e.* 2 Hz [53,54]). Indeed, in our preliminary tests, we observed a significant increase in the temperature of the saline solution when the test lasted longer than 15 h. The increase in temperature could go beyond 37 °C, which is higher than the body temperature, for the samples tested at the frequency of 2 Hz. Therefore, we chose 10 Hz load frequency to avoid the significant change of temperature during fatigue loading. The tolerated change in the temperature was 2 K for these fatigue tests.

Specimens were randomly chosen for being tested in the fatigue loading, and various force amplitudes were considered for such tests. Four levels of force amplitude, F_n , (*i.e.*, 360, 450, 540 and 720 N) were chosen. These values were selected to be below the yield forces determined in monotonic compression tests. Compressive cyclic loading was determined by the force amplitude, $F_n = \frac{F_{max} - F_{min}}{2}$, the mean force, $F_m = \frac{F_{max} + F_{min}}{2}$, and the force ratio, $R = \frac{F_{min}}{F_{max}} = 0.1$, where F_{max} , and F_{min} were the maximum and minimum force, respectively.

From μ CT imaging, the nominal area, $A_{n,i}$, calculated by using the diameter at i^{th} stack of the image, and relative bone density, BV/TV_i at the same i^{th} stack were calculated. Thereafter, for each stack of the image the effective area was calculated as $A_{eff,i} = A_{n,i} \times BV/TV_i$. That led to the definition of the nominal stress, $\sigma_n = \frac{F}{A_n}$, and the effective

stress, $\sigma_{eff} = \frac{F}{A_{eff}}$, where $A_n = \min\{A_{n,i}\}$ and $A_{eff} = \min\{A_{eff,i}\}$. The nominal and the effective stress amplitudes were calculated as $\sigma_{a,n} = \frac{F_{max} - F_{min}}{2A_n}$ and $\sigma_{a,eff} = \frac{F_{max} - F_{min}}{2A_{eff}}$, respectively.

The longitudinal strain was defined as $\epsilon = \frac{\delta}{L_{eff}}$, where δ is the measured displacement from the actuator linear variable differential transformer (LVDT). We performed a preliminary study where we removed the saline solution tank and attached an extensometer (MTS 632.26F-23) to the specimen. In this test, the bone sample had a total length of 25 mm, whereas the extensometer on the specimen was installed over a length of 8 mm. The comparison between the axial strain, obtained from the direct measurement of the extensometer, and the axial strain, obtained from LVDT, showed a 3.5% difference. It was not possible to install an extensometer due to space constraints in the experimental set-up. During the fatigue loading, the displacement amplitude varied from 0.05 to 0.10 mm, on the edge of the resolution of the LVDT (0.01 mm).

The elastic modulus was calculated as follows, $E_i = \frac{\sigma_{max} - \sigma_{min}}{\epsilon_{max} - \epsilon_{min}} = \frac{F_{max} - F_{min}}{\delta_{max} - \delta_{min}} \times \frac{L_{eff}}{A_{eff}} = \frac{K_i L_{eff}}{A_{eff}}$, where K_i is the stiffness at the i^{th} hysteresis loop, measured from the slope of the force-displacement curve, between the maximum and minimum force, and the corresponding displacement at that hysteresis loop, and $\bar{A}_{eff} = \text{mean}\{A_{eff}\}$. The initial elastic modulus, E_0 , was calculated with the average effective bone area, \bar{A}_{eff} , since the total material response for the overall displacement of the sample was measured. The accumulation of damage at the i^{th} hysteresis cycle, D_i , was calculated as $D_i = 1 - \frac{E_i}{E_0}$.

Fatigue tests were stopped either when the maximum displacement reached 2 mm or when the cycles exceeded $N > 8 \times 10^5$. Force, displacement, and time were recorded from the machine with a sampling rate of 10 measurements per second. During testing, the temperature of the saline solution was kept approximatively constant (34–36 °C). Finally, 21 specimens were tested under fully compressive fatigue loading.

2.3.3. Interrupted fatigue tests

In the interrupted fatigue testing, we stopped each test twice before reaching the life cycle end-condition. Three levels of force amplitude, *i.e.*, 360, 450, and 540 N (equivalent to nominal stress amplitude of $\sigma_n = 2.37, 2.96, \text{ and } 3.56$ MPa, respectively) were selected. We adopted a cycle-based stop criterion depending on the chosen force amplitude: $N_{stop} = 1 \times 10^3$, for $F = 360$ N; $N_{stop} = 3.6 \times 10^3$, for $F = 450$ N; $N_{stop} = 2.4 \times 10^5$, for $F = 540$ N. At each stopping point, clinical and morphological parameters were measured via DXA and μ CT, respectively, following the protocols described in Sections 2.2.1 and 2.2.2. Six specimens were tested for the interrupted cyclic loading, *i.e.*, two specimens per each force level. The total number of life cycles was then added to the data of fatigue life testing. Therefore, the total number of the specimens considered for the fatigue curve is 27.

2.4. Statistical analysis

A balanced Latin square approach was used for the design of mechanical fatigue testing. Statistical analysis was carried out in MATLAB® (R2015a) and SAS 9.2, and a p -value < 0.05 was assumed as the significant level.

3. Results and discussion

3.1. Fatigue life

Descriptive statistical data for morphological and clinical parameters for the pooled data are given in Table 1. Fig. 1a shows the S-N curve of the trabecular bone samples, considering the nominal stress amplitude, $\sigma_{a,n}$, and the number of loading cycles to failure, N_f . The pooled data are given in Table 2. It is evident that the obtained data are

Table 1
The mean \pm standard deviation for the clinical and morphological parameters of pooled data.

Morphological parameters	
BV/TV [%]	43.60 \pm 3.66
BS/TV [1/mm]	4.10 \pm 0.36
BS/BV [1/mm]	9.44 \pm 0.91
Tb. Th [mm]	0.27 \pm 0.03
Tb. EF	-0.03 \pm 0.03
Conn. D [1/mm ³]	2.78 \pm 1.02
DA [-]	0.52 \pm 0.09
Clinical parameters	
BMD [g/cm ²]	0.38 \pm 0.05
TBS	1.03 \pm 0.14

scattered and do not have any specific trend across the loading cycles. To obtain a suitable description of the fatigue behavior of trabecular bone, we defined an effective area, A_{eff} , which takes into account the porosity of the bone tissue and, consequently, allowed us to evaluate an

Table 2
The mean, standard deviation (SD), minimum and maximum for the initial elastic stiffness, E_0 , stress amplitude, σ_a , fatigue life, N_f , and accumulated damage, D_f .

	Mean	SD	Minimum	Maximum
E_0 [MPa]	2360	340	1700	3030
σ_a [MPa]	10	3.1	5.7	17.7
N_f	1.4×10^5	-	1	8.0×10^5
D_f	0.39	0.07	0.24	0.50

effective stress, $\sigma_{a,eff}$. We normalized the effective stress amplitude to the initial elastic stiffness of each specimen. The resulting normalized stress vs. life ($\frac{\sigma_{a,eff}}{E_0} - N_f$) trend is depicted in Fig. 1b, together with the literature trends [21,31]. The comparison in Fig. 1b shows similar fatigue life behavior for human, bovine, and porcine trabecular bone, which follow the relationship $\frac{\sigma_{a,eff}}{E_0} = aN_f^b$ with $a = -0.01$ and $b = -0.1$ ($R^2 = 83.34\%$, $p < 0.001$) (Fig. 1b). The porcine results are, however,

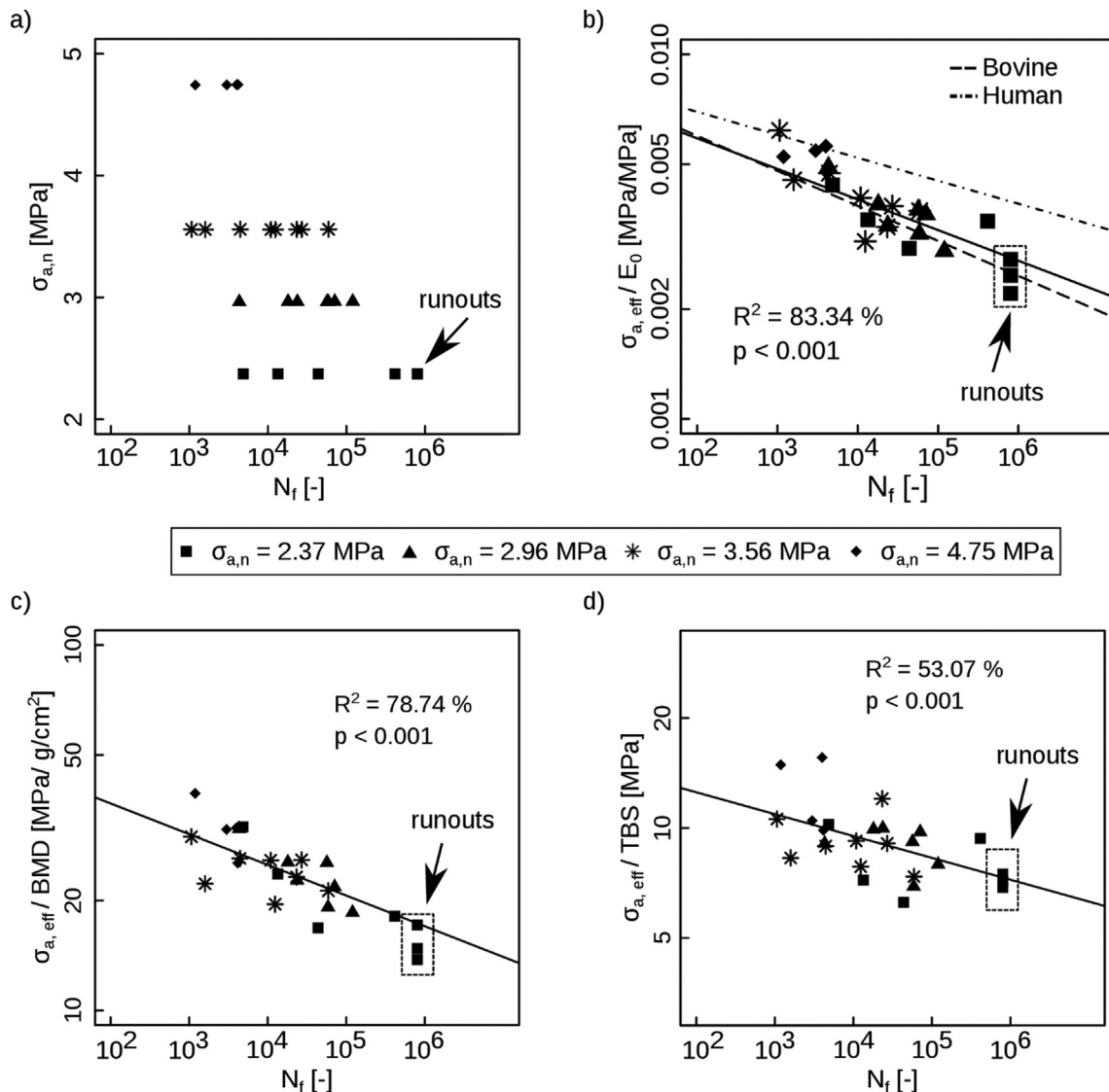


Fig. 1. (a) Semi-log plot of four force (nominal stress) amplitudes applied for the prediction of the fatigue life. (b) Fatigue life curve for the normalized stress amplitude with respect to the initial elastic modulus and its comparison with fatigue life of bovine trabecular [21] and human vertebrae [31]. The plot is shown in log-log and $a = -0.01$, $b = -0.1$ are the regression coefficients for $\frac{\sigma_{a,eff}}{E_0} = aN_f^b$ (solid line). Three samples tested at the nominal stress amplitude $\sigma_{a,n} = 2.37$ MPa did not fail after 1 million cycles (runouts). The ratio of stress amplitude to the BMD (c) and TBS (d) exhibit a significant correlation with the fatigue life of the porcine trabecular bone.

closer to the bovine ones.

We also calculated the stress amplitudes based on the mean effective area, $A_{eff,mean}$, and the nominal area, $A_{nominal}$, of the trabecular specimens (Fig. S2 of the supplementary document). We found a higher correlation between the normalized stress amplitudes and the fatigue life of the trabecular bone when considering the minimum effective area (Figs. 1b and S2 of the supplementary document).

Several authors [21,27,30,32,55,56] have shown similar evidence of fatigue life trend for trabecular bone under compressive loading. The proposed models are based on Coffin-Manson equations, for low-cycle fatigue, and Wöhler or Basquin equations, for high-cycle fatigue. In some cases, the authors considered the F-N trend [27,32] and normalized the force with respect to the ultimate tensile strength [27] or with respect to different correction factors (i.e., sample area, sample strength estimation based on age and BMD, and applied load) [32]. In other cases, the authors considered the S-N curve and normalized the nominal stress by the pre-fatigue elastic modulus [31]. Instead, we proposed a model based on the effective stress, $\sigma_{a,eff}$, which showed a significant correlation with the fatigue life cycles. Similar normalizations were performed with respect to BMD (Fig. 1c) and TBS (Fig. 1d), where the effective stresses showed a significant correlation with the fatigue life cycles. The linear regression showed a significant correlation between BMD and the life cycles (Fig. 2a) and no correlation between TBS and the life cycles was observed (Fig. 2b).

3.2. Failure modes and failure region

We observed three principal types of fracture: (i) a diagonal fracture, generally occurring in the top region of the sample and being 45°-oriented (Fig. 3a), (ii) an orthogonal fracture to the longitudinal direction, generally occurring in the mid-region of the sample (Fig. 3b), and (iii) a splitting fracture, generally occurring as a lateral separation of part of the trabecular bone sample, causing a buckling-like failure (Fig. 3c). These failure modes are in agreement with previous findings in literature [57]. In particular, the transverse failure represents a brittle-like failure and is generally associated with trabeculae orthogonally oriented to the loading direction. A diagonal failure can be considered as a ductile-like failure. Buckling-like failure, instead, is common to oblique trabeculae and may cause a longitudinal splitting.

We calculated the BV/TV trend along with the specimen height, L_{eff} ,

and showed its changes during the interrupted fatigue tests (Fig. 4). We noticed that the location of the catastrophic failure corresponds to the zone with the lowest BV/TV value (Fig. 4a). This finding also shows agreement with a previous literature study [58]. After the final rupture, the BV/TV increased suddenly in the region where the failure occurred, while its value remained almost constant in other parts of the specimen (Fig. 4b). This can be explained as trabecular bone can recover large amounts of deformation after an overload [59–61].

3.3. Variation of the clinical, morphological, and mechanical parameters

The local increase in BV/TV, caused by failure (i.e., the local collapse of the struts), also increased the mean value of BV/TV for each specimen. This finding is in line with the experimental results of our previous study where different morphometric parameters of pre- and post- quasi-static damage were measured in porcine trabecular bone [62]. This trend is more obvious for all the specimens subjected to the interrupted fatigue testing (Fig. 5a): failure always corresponds to an increase in BV/TV. In particular, we measured an increase (about 20%) in the BV/TV between the failed samples and the undamaged ones. A 20% decrease in *Conn. D* was observed after a catastrophic failure (Fig. 5b), which confirms the local breakage of the trabeculae and the damage accumulation under cyclic loading. The drop in *Conn. D* with increasing life cycles and damage was almost consistent for all the specimens. As expected, we did not observe any change in BMD (Fig. 5c) as we prevented any chemical deterioration during fatigue loading by keeping the specimen in wet conditions. TBS seemed decreasing (Fig. 5d), which is consistent with the *Conn. D*. trend. Both the TBS and the *Conn. D*. can be considered morphometric parameters, which provide information on bone microarchitecture. Indeed, according to previous studies, there is a correlation between TBS and *Conn. D*., where high values of both indicate the presence of a better skeletal tissue, whereas low values are a symptom of a weaker skeletal texture or a degraded microarchitecture [63,64]. However, being TBS obtained from BMD, it is limited by its two-dimensional nature and cannot capture the three-dimensional microarchitecture. Besides, TBS is affected by the size and position of the samples [65,66]. These limitations could explain the non-clear trend observed for the TBS with respect to the *Conn. D*.

The stiffness degradation was measured during the interrupted

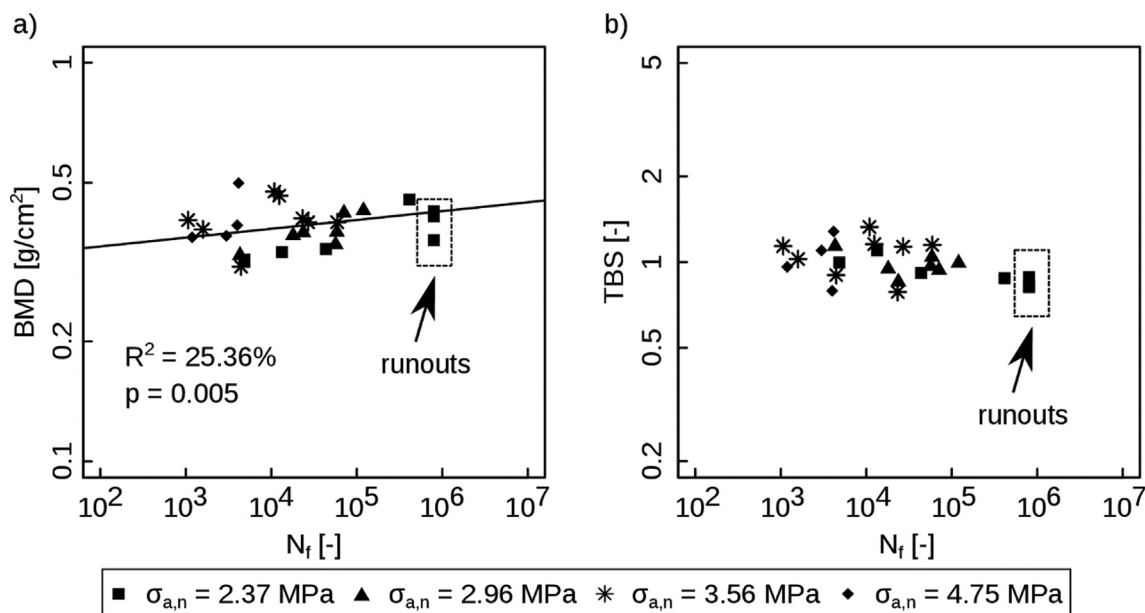


Fig. 2. Clinical parameters BMD (a) and TBS (b) and the fatigue life cycles shown in the log-log form. A significant linear correlation was found between BMD and fatigue life cycle while no significant correlation was found for TBS vs. fatigue life cycle.

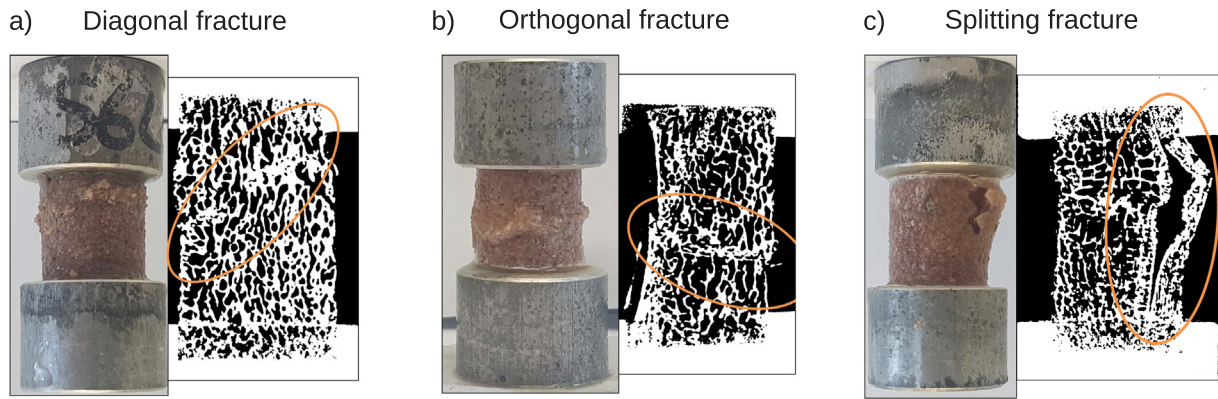


Fig. 3. Three different failure modes were observed in the mechanical fatigue loading where either oblique or straight macroscopic cracks propagated in the trabecular bones. The position of the fracture generally occurred at the top (a), center (b), or the lateral part (c) of the specimens.

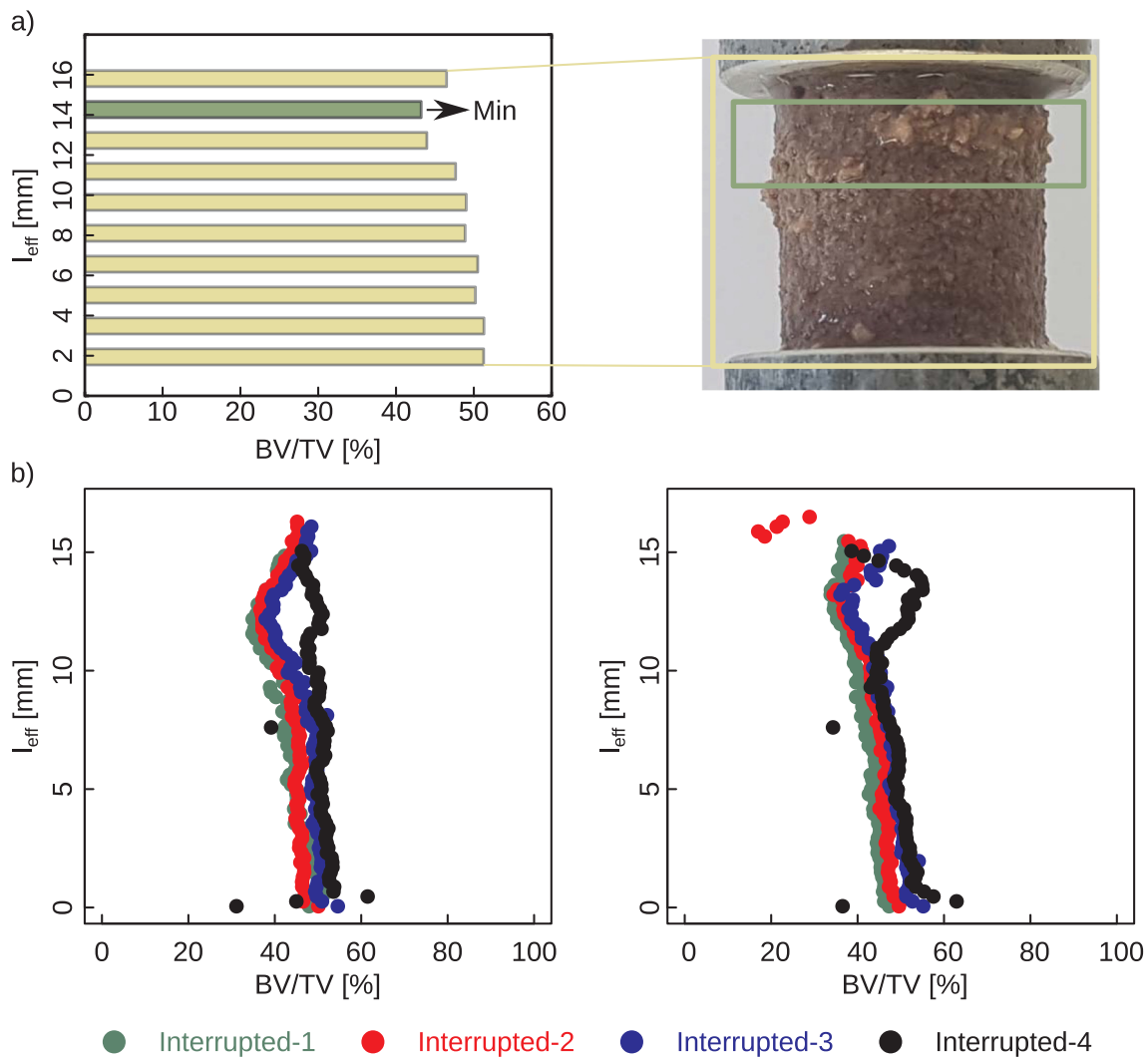


Fig. 4. (a) The distribution of the BV/TV along with the effective length of the specimen, l_{eff} before testing (left) and fractured specimen under interrupted fatigue tests. The fracture starts at the zones with the lowest BV/TV. (b) BV/TV trend through the effective length between the grips, L_{eff} , after different interrupted cyclic loading, the local BV/TV increased after a catastrophic failure in the weakest regions. BV/TV was calculated as an average of every eight stacks of images from μ CT images. The interrupted-1, 2, 3 and 4 refer to the number of cycles at which the fatigue tests were stopped.

fatigue loading, providing a mechanical damage parameter, D (Table 2). Our results showed the bone samples reached about 50% damage at the end of the interrupted tests (Fig. 5e). Different models have been used, in the literature, for the prediction of the accumulated damage vs. life cycles, such as those proposed by Chaboche [67], Griffin

et al. [68] and Pattin et al. [22]. These models showed that the (rate of) damage accumulation in bones could also be influenced by the level of applied cyclic stresses [69,70] and other geometrical features of bone [71,70]. From our experimental results, we found out that the level of applied cyclic stress could affect the rate of damage as fatigue cycles

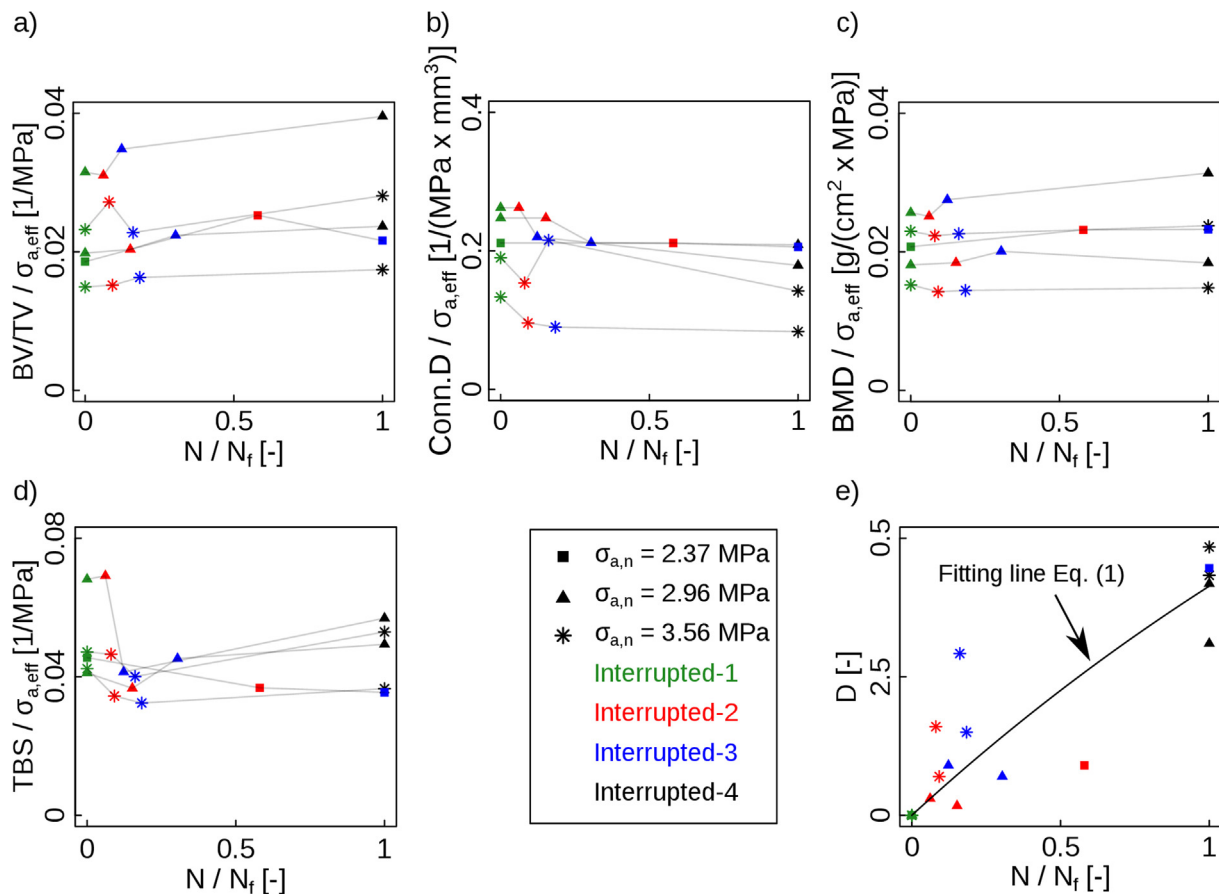


Fig. 5. Change in (a) BV/TV, (b) connectivity (c) BMD, (d) TBS and (e) accumulation of damage in the interrupted mechanical fatigue tests for five different samples under various force amplitudes and life fraction, $\frac{N}{N_f}$. The grey lines for (a–d) show the changes in the corresponding parameter in one specimen and are plotted to guide the eye. To eliminate the effect of load levels, the parameters in (a–d) are normalized to the effective stresses. The fitting line in (e) is based on Eq. (1).

progressed. We calculated the parameters of the damage model using a similar procedure to the one proposed by Griffin et al. [68] for the prediction of damage in the interstitial bone of cortical tissue (Eq. (1)):

$$D = k_2 \sigma_a^q [1 - \exp(-k_1 (N/N_f))] \quad (1)$$

where $k_2 = 0.62$, $k_1 = 0.36$, $q = 0.36$ are coefficients of the model obtained from the non-linear least square fit on the interrupted fatigue tests (Fig. 5e).

In this study, we measured an average BMD and TBS for each specimen and did not include the local variation of these measurements. This is due to the nature of the current densitometry technique that provides us average values. These results could be useful for life prediction if the microstructures of bone were uniformly distributed. The heterogeneity of BMD and its effect on the fatigue life of vertebra have been shown in a previous study [72], suggesting that a local BMD and a local minimum of BV/TV [58] could provide a better representation of the fatigue life estimation of trabecular bone.

The testing protocol used in this study was similar to those proposed in the literature [21,2,20,32,31,73] for the mechanical fatigue testing of trabecular bones. Therefore, during the fatigue testing, the trabecular specimens were kept in the normal saline solution. We did not quantitatively measure whether keeping the bone specimens in such solution during the fatigue testing could chemically degrade bones or influence their mechanical properties. Recent study has shown that storing bones for less than 3 days in the saline solution does not significantly affect the mechanical properties of bone [74]. From our results we also did not observe a significant change in BMD before and after testing showing no significant change in the chemical composition of bones.

Although it has been shown that microcracks are significantly

correlated to the fatigue life of cancellous bone [2], we did not quantify the accumulated microdamage under fatigue loading owing to the intrinsic limitations of our instruments. Indeed, the micro damage cannot be captured by the clinical measurements as the microcrack average length is less than 100 μm [75–77], which is below the resolution of DXA images. The fatigue-induced microdamage generally accumulates in the older interstitial part of the cancellous bone and form longer microcracks [20]. Our results evidenced that other diagnostic methods, such as microindentation [78,79] and high resolution quantitative computed tomography (HRQCT), are required for the invasive detection of microdamage in bone [80].

4. Conclusion

This study aimed at investigating the effect of fatigue-induced damage on bone microarchitecture and the characteristic bone clinical parameters, by combining fatigue testing on *ex-vivo* porcine trabecular bone samples, DXA measurements, and μCT imaging.

- The predictive model for the description of the fatigue life of trabecular bone was obtained considering the specimen-specific effective area—measured by μCT —and the BMD showed a good comparison with recent literature results.
- The μCT imaging showed that the sub-regions with minimum BV/TV values are better predictors of the location of mechanical failure in trabecular bone than averaged-specimen BV/TV values, confirming that failure is a local phenomenon.
- Interrupted cyclic loading coupled with μCT showed that damage accumulation occurs locally, causing a sudden increase in the local

and global BV/TV and a drop in *Conn. D* with increasing life. The local variations of bone volume fraction and bone micro-architecture, calculated from μ CT images, suggest a need for the introduction of local sensitive parameters for BMD and TBS rather than an average value.

The outcome of this study suggests that the current invasive and non-invasive diagnosis protocols, *i.e.*, μ CT and DXA, respectively, are not able to quantify the fatigue-induced damage. Fatigue-induced damage is a local phenomenon, and for its characterization new local parameters, able to detect punctual variations of bone mass and microarchitecture, need to be defined and validated.

Declaration of Competing Interest

The authors declare that they have no known competing financial interests or personal relationships that could have appeared to influence the work reported in this paper.

Acknowledgements

The authors would like to thank Prof Michele Carboni, for helping in μ CT imaging, Lorenzo Giudici, for helping in mechanical testing, and “SMT Laboratorio Prove e Officine Meccaniche” for helping in specimen cutting.

Appendix A. Supplementary material

Supplementary data to this article can be found online at <https://doi.org/10.1016/j.ijfatigue.2019.105451>.

References

- Breer S, Krause M, Marshall RP, Oheim R, Amling M, Barvencik F. Stress fractures in elderly patients. *Int Orthop* 2012;36(12):2581–7.
- Lambers FM, Bouman AR, Rinnac CM, Hernandez CJ. Microdamage caused by fatigue loading in human cancellous bone: relationship to reductions in bone biomechanical performance. *PLoS ONE* 2013;8(12):e83662.
- Taylor D, Hazenberg JG, Lee TC. Living with cracks: damage and repair in human bone. *Nat Mater* 2007;6(4):263.
- Moreira CA, Bilezikian JP. Stress fractures: concepts and therapeutics. *J Clin Endocrinol Metab* 2016;102(2):525–34.
- Acevedo Claire, Stadelmann Vincent A, Pioletti Dominique P, Alliston Tamara, Ritchie Robert O. Fatigue as the missing link between bone fragility and fracture. *Nat Biomed Eng* 2018;2(2):62–71. <https://doi.org/10.1038/s41551-017-0183-9>.
- Iwamoto J, Takeda T. Stress fractures in athletes: review of 196 cases. *J Orthopaedic Sci* 2003;8(3):273–8.
- Sormaal MJ, Niva MH, Kiuru MJ, Mattila VM, Pihlajamäki HK. Bone stress injuries of the talus in military recruits. *Bone* 2006;39(1):199–204.
- Burr DB, Forwood MR, Fyhrie DP, Martin RB, Schaffler MB, Turner CH. Bone microdamage and skeletal fragility in osteoporotic and stress fractures. *J Bone Miner Res* 1997;12(1):6–15.
- Burr DB, Turner CH, Naick P, Forwood MR, Ambrosius W, Hasan MS, et al. Does microdamage accumulation affect the mechanical properties of bone? *J Biomech* 1998;31(4):337–45.
- Fang G, Ji B, Liu XS, Guo XE. Quantification of trabecular bone microdamage using the virtual internal bond model and the individual trabeculae segmentation technique. *Comput Methods Biomech Biomed Eng* 2010;13(5):605–15.
- Keaveny TM, Wachtel EF, Guo XE, Hayes WC. Mechanical behavior of damaged trabecular bone. *J Biomech* 1994;27(11):1309–18.
- Lee TC, O'Brien FJ, Gunnlaugsson T, Parkesh R, Taylor D. Microdamage and bone mechanobiology. *Technol Health Care* 2006;14:359–65.
- Mirzaali MJ, Libonati F, Vena P, Mussi V, Vergani L, Strano M. Investigation of the effect of internal pores distribution on the elastic properties of closed-cell aluminum foam: a comparison with cancellous bone. *Proc Struct Integr* 2016;2:1285–94.
- Mirzaali MJ, Mussi V, Vena P, Libonati F, Vergani L, Strano M. Mimicking the loading adaptation of bone microstructure with aluminum foams. *Mater Des* 2017;126:207–18.
- Nagaraja S, Couse TL, Gulberg RE. Trabecular bone microdamage and microstructural stresses under uniaxial compression. *J Biomech* 2005;38(4):707–16.
- Wang X, Niebur GL. Microdamage propagation in trabecular bone due to changes in loading mode. *J Biomech* 2006;39:781–90.
- Wolfram U, Wilke H-J, Zysset PK. Damage accumulation in vertebral trabecular bone depends on loading mode and direction. *J Biomech* 2011;44(6):1164–9.
- Dendorfer S, Maier H, Taylor D, Hammer J. Anisotropy of the fatigue behaviour of cancellous bone. *J Biomech* 2008;41(3):636–41.
- Diab T, Sit S, Kim D, Rho J, Vashishth D. Age-dependent fatigue behaviour of human cortical bone. *Eur J Morphol* 2005;42(1–2):53–9.
- Goff M, Lambers F, Nguyen T, Sung J, Rinnac C, Hernandez C. Fatigue-induced microdamage in cancellous bone occurs distant from resorption cavities and trabecular surfaces. *Bone* 2015;79:8–14.
- Moore TL, Gibson LJ. Fatigue of bovine trabecular bone. *J Biomech Eng* 2003;125(6):761–8.
- Pattin C, Caler W, Carter D. Cyclic mechanical property degradation during fatigue loading of cortical bone. *J Biomech* 1996;29(1):69–79.
- García D, Zysset PK, Charlebois M, Curnier A. A three-dimensional elastic plastic damage constitutive law for bone tissue. *Biomech Model Mechanobiol* 2009;8(2):149–65.
- Keaveny TM, Wachtel EF, Zadesky SP, Arramon YP. Application of the tsai-wu quadratic multiaxial failure criterion to bovine trabecular bone. *J Biomech Eng* 1999;121(1):99–107.
- Mirzaali MJ, Bürki A, Schwiedrzik J, Zysset PK, Wolfram U. Continuum damage interactions between tension and compression in osteonal bone. *J Mech Behav Biomed Mater* 2015;49:355–69.
- Zysset PK, Curnier A. A 3d damage model for trabecular bone based on fabric tensors. *J Biomech* 1996;29:1549–58.
- Brinckmann P, Biggemann M, Hilweg D. Fatigue fracture of human lumbar vertebrae. *Clin Biomech* 1988;3:i–23.
- Caler WE, Carter DR. Bone creep-fatigue damage accumulation. *J Biomech* 1989;22(6–7):625–35.
- Carter DR, Caler WE, Spengler DM, Frankel VH. Fatigue behavior of adult cortical bone: the influence of mean strain and strain range. *Acta Orthop Scand* 1981;52(5):481–90.
- Schaffler M, Radin E, Burr D. Long-term fatigue behavior of compact bone at low strain magnitude and rate. *Bone* 1990;11(5):321–6.
- Haddock SM, Yeh OC, Mummaneni PV, Rosenberg WS, Keaveny TM. Similarity in the fatigue behavior of trabecular bone across site and species. *J Biomech* 2004;37(2):181–7.
- Huber G, Nagel K, Skrzypiec DM, Klein A, Püschel K, Morlock MM. A description of spinal fatigue strength. *J Biomech* 2016;49(6):875–80.
- Silva BC, Leslie WD, Resch H, Lamy O, Lesnyak O, Binkley N, et al. Trabecular bone score: a noninvasive analytical method based upon the dxa image. *J Bone Miner Res* 2014;29(3):518–30.
- Ulivieri FM, Silva BC, Sardanelli F, Hans D, Bilezikian JP, Caudarella R. Utility of the trabecular bone score (tbs) in secondary osteoporosis. *Endocrine* 2014;47(2):435–48.
- Bousson V, Bergot C, Sutter B, Levitz P, Cortet B, et al. Trabecular bone score (tbs): available knowledge, clinical relevance, and future prospects. *Osteoporos Int* 2012;23(5):1489–501.
- Silva BC, Broy SB, Boutroy S, Schousboe JT, Shepherd JA, Leslie WD. Fracture risk prediction by non-bmd dxa measures: the 2015 iscd official positions part 2: trabecular bone score. *J Clin Densitomet* 2015;18(3):309–30.
- Blake GM, Fogelman I. The role of dxa bone density scans in the diagnosis and treatment of osteoporosis. *Postgrad Med J* 2007;83(982):509–17.
- Hunt HB, Donnelly E. Bone quality assessment techniques: Geometric, compositional, and mechanical characterization from macroscale to nanoscale. *Clin Rev Bone Mineral Metab* 2016;14(Sep):133–49.
- Hui SL, Slemenda CW, Johnston CC. Age and bone mass as predictors of fracture in a prospective study. *J Clin Investig* 1988;81(6):1804–9.
- Martin RM, Correa PHS. Bone quality and osteoporosis therapy. *Arquivos Brasileiros de Endocrinologia & Metabologia* 2010;54(2):186–99.
- Schuit S, Van der Klift M, Weel A, De Laet C, Burger H, Seeman E, et al. Fracture incidence and association with bone mineral density in elderly men and women: the rotterdam study. *Bone* 2004;34(1):195–202.
- Allolio B. Risk factors for hip fracture not related to bone mass and their therapeutic implications. *Osteoporos Int* 1999;9(8):S9–17.
- Ritchie Robert O, Buehler Markus J, Hansma Paul. Plasticity and toughness in bone. *Phys Today* 2009;62(6):41–7. <https://doi.org/10.1063/1.3156332>.
- Busscher I, Ploegmakers JJ, Verkerke GJ, Veldhuizen AG. Comparative anatomical dimensions of the complete human and porcine spine. *Eur Spine J* 2010;19(7):1104–14.
- Abramoff M, Magelhaes P, Ram S. Image processing with imagej. *Biophoton Int* 2004;11(7):36–42.
- Doube M, Kosowski MM, Arganda-Carreras I, Cordelières FP, Dougherty RP, Jackson JS, et al. Free and extensible bone image analysis in ImageJ. *Bone* 2010;47(6):1076–9.
- Otsu N. A threshold selection method from gray-level histograms. *IEEE Trans Syst, Man, Cybernet* 1979;9(1):62–6.
- Hildebrand T, Rüegsegger P. A new method for the model-independent assessment of thickness in three-dimensional images. *J Microsc* 1997;185(1):67–75.
- Lorensen WE, Cline HE. Marching cubes: A high-resolution 3d surface construction algorithm. *SIGGRAPH Comput Graph* 1987;21(4):163–9.
- Doube M. The ellipsoid factor for quantification of rods, plates, and intermediate forms in 3d geometries. *Front Endocrinol* 2015;6.
- Rietbergen Bv, Odgaard A, Kabel J, Huisjes R. Relationships between bone morphology and bone elastic properties can be accurately quantified using high-resolution computer reconstructions. *J Orthop Res* 1998;16:23–8.
- Whitehouse WJ. The quantitative morphology of anisotropic trabecular bone. *J Microsc* 1974;101(2):153–68.
- Ji T, Pachi A. Frequency and velocity of people walking. *Struct Eng* 2005;84(3):36–40.

- [54] Lafferty J, Raju P. The influence of stress frequency on the fatigue strength of cortical bone. *J Biomech Eng* 1979;101(2):112-3.
- [55] Bowman S, Guo X, Cheng D, Keaveny T, Gibson L, Hayes W, et al. Creep contributes to the fatigue behavior of bovine trabecular bone. *J Biomech Eng* 1998;120(5):647-54.
- [56] Fatihhi S, Harun M, Kadir MRA, Abdullah J, Kamarul T, Öchsner A, et al. Uniaxial and multiaxial fatigue life prediction of the trabecular bone based on physiological loading: a comparative study. *Ann Biomed Eng* 2015;43(10):2487-502.
- [57] Michel MC, Guo X-DE, Gibson LJ, McMahon TA, Hayes WC. Compressive fatigue behavior of bovine trabecular bone. *J Biomech* 1993;26(4-5):453-63.
- [58] Nazarian A, Stauber M, Zurakowski D, Snyder BD, Müller R. The interaction of microstructure and volume fraction in predicting failure in cancellous bone. *Bone* 2006;39(6):1196-202.
- [59] Keaveny TM, Wachtel EF, Kopperdahl DL. Mechanical behavior of human trabecular bone after overloading. *J Orthop Res* 1999;17(3):346-53.
- [60] Fyhrie DP, Schaffler MB. Failure mechanisms in human vertebral cancellous bone. *Bone* 1994;15(1):105-9.
- [61] Torres AM, Matheny JB, Keaveny TM, Taylor D, Rimnac CM, Hernandez CJ. Material heterogeneity in cancellous bone promotes deformation recovery after mechanical failure. *Proc Natl Acad Sci* 2016;113(11):2892-7.
- [62] Mirzaali MJ, Libonati F, Ferrario D, Rinuado LC, Messina F, Ulivieri BM, et al. Determinants of bone damage: an ex-vivo study on porcine vertebrae. *PLoS ONE* 2018;13(8):e0202210.
- [63] Muschitz C, Kocian R, Haschka J, Pahr D, Kaider A, Pietschmann P, et al. Tbs reflects trabecular microarchitecture in premenopausal women and men with idiopathic osteoporosis and low-traumatic fractures. *Bone* 2015;79:259-66.
- [64] Pothuaud L, Barthe N, Krieg M-A, Mehsen N, Carceller P, Hans D. Evaluation of the potential use of trabecular bone score to complement bone mineral density in the diagnosis of osteoporosis: a preliminary spine bmd-matched, case-control study. *J Clin Densitom* 2009;12(2):170-6.
- [65] Bolotin H. Dxa in vivo bmd methodology: an erroneous and misleading research and clinical gauge of bone mineral status, bone fragility, and bone remodelling. *Bone* 2007;41(1):138-54.
- [66] Nishiyama KK, Shane E. Clinical imaging of bone microarchitecture with hr-pqct. *Curr Osteop Report* 2013;11(2):147-55.
- [67] Chaboche J-L. Continuous damage mechanics a tool to describe phenomena before crack initiation. *Nucl Eng Des* 1981;64(2):233-47.
- [68] Griffin L, Gibeling J, Martin R, Gibson V, Stover S. Model of flexural fatigue damage accumulation for cortical bone. *J Orthop Res* 1997;15(4):607-14.
- [69] Campbell AM, Cler ML, Skurla CP, Kuehl JJ. Damage accumulation of bovine bone under variable amplitude loads. *Bone Reports* 2016;5:320-32.
- [70] Varvani-Farahani A, Najmi H. A damage assessment model for cadaveric cortical bone subjected to fatigue cycles. *Int J Fatigue* 2010;32(2):420-7.
- [71] Cotton JR, Winwood K, Zioupos P, Taylor M. Damage rate is a predictor of fatigue life and creep strain rate in tensile fatigue of human cortical bone samples. *J Biomech Eng* 2005;127(2):213-9.
- [72] Yeni YN, Poisson LM, Flynn MJ. Heterogeneity of bone mineral density and fatigue failure of human vertebrae. *J Biomech* 2013;46(7):1396-9.
- [73] Kim J, Niinomi M, Akahori T, Toda H. Fatigue properties of bovine compact bones that have different microstructures. *Int J Fatigue* 2007;29(6):1039-50.
- [74] Zhang G, Deng X, Guan F, Bai Z, Cao L, Mao H. The effect of storage time in saline solution on the material properties of cortical bone tissue. *Clin Biomech* 2018;57:56-66.
- [75] Burr DB, Stafford T. Validity of the bulk-staining technique to separate artifactual from in vivo bone microdamage. *Clin Orthop Relat Res* 1990;260:305-8.
- [76] Landrigan MD, Li J, Turnbull TL, Burr DB, Niebur GL, Roeder RK. Contrast-enhanced micro-computed tomography of fatigue microdamage accumulation in human cortical bone. *Bone* 2011;48(3):443-50.
- [77] Wolfram U, Schwiedrzik JJ, Mirzaali M, Bürki A, Varga P, Olivier C, et al. Characterizing microcrack orientation distribution functions in osteonal bone samples. *J Microsc* 2016;264(3):268-81.
- [78] Diez-Perez A, Güerri R, Nogues X, Cáceres E, Pena MJ, Mellibovsky L, et al. Microindentation for in vivo measurement of bone tissue mechanical properties in humans. *J Bone Miner Res* 2010;25(8):1877-85.
- [79] Mirzaali MJ, Schwiedrzik JJ, Thaiwichai S, Best JP, Michler J, Zysset PK, et al. Mechanical properties of cortical bone and their relationships with age, gender, composition and microindentation properties in the elderly. *J Bone* 2015.
- [80] Graeff C, Marin F, Petto H, Kayser O, Reisinger A, Peña J, et al. High resolution quantitative computed tomography-based assessment of trabecular microstructure and strength estimates by finite-element analysis of the spine, but not dxa, reflects vertebral fracture status in men with glucocorticoid-induced osteoporosis. *Bone* 2013;52(2):568-77.